ORIGINAL RESEARCH REPORT

In vitro and in vivo study on the osseointegration of BCP-coated versus uncoated nondegradable thermoplastic polyurethane focal knee resurfacing implants

Ralph M. Jeuken[1] | Alex K. Roth[1] | Marloes J.M. Peters[1] | Tim J.M. Welting[1] | Lodewijk W. van Rhijn[1] | Jac Koenen[2] | Ruud J.R.W. Peters[2] | Jens C. Thies[2] | Pieter J. Emans[1]

[1]Department of Orthopaedic Surgery, Research School CAPHRI, Maastricht University Medical Center, Maastricht, The Netherlands

[2]DSM Biomedical BV, Geleen, The Netherlands

Correspondence
Pieter J. Emans, Maastricht University Medical Center, Department of Orthopedic Surgery, Research School CAPHRI, P. Debyelaan 25, 6229 HX, Maastricht, The Netherlands.
Email: p.emans@mumc.nl

Funding information
Inscite Biomedical

Abstract

Focal knee resurfacing implants (FKRIs) are intended to treat cartilage defects in middle-aged patients. Most FKRIs are metal-based, which hampers follow-up of the joint using magnetic resonance imaging and potentially leads to damage of the opposing cartilage. The purpose of this study was to develop a nondegradable thermoplastic polyurethane (TPU) FKRI and investigate its osseointegration. Different surface roughness modifications and biphasic calcium phosphate (BCP) coating densities were first tested in vitro on TPU discs. The in vivo osseointegration of BCP-coated TPU implants was subsequently compared to uncoated TPU implants and the titanium bottom layer of metal control implants in a caprine model. Implants were implanted bilaterally in stifle joints and animals were followed for 12 weeks, after which the bone-to-implant contact area (BIC) was assessed. Additionally, 18F-sodium-fluoride (18F-NaF) positron emission tomography PET/CT-scans were obtained at 3 and 12 weeks to visualize the bone metabolism over time. The BIC was significantly higher for the BCP-coated TPU implants compared to the uncoated TPU implants (p = .03), and did not significantly differ from titanium (p = .68). Similar 18F-NaF tracer uptake patterns were observed between 3 and 12 weeks for the BCP-coated TPU and titanium implants, but not for the uncoated implants. TPU FKRIs with surface modifications could provide the answer to the drawbacks of metal FKRIs.

KEYWORDS
bone ingrowth, coatings, implant interface, polyurethanes

1 | INTRODUCTION

Cartilage defects are highly prevalent in patients over 40 years of age (Curl et al., 1997), and may lead to severe impairment of quality of life

(Heir et al., 2010, 2017). Moreover, cartilage defects are a major independent risk factor for total knee arthroplasty (TKA) (Everhart, Abouljoud, Kirven, & Flanigan, 2019). A survey amongst orthopaedic surgeons reveals a perceived treatment gap for cartilage defect repair in the middle-aged patient population (i.e., 40–60 years) (Li, Karlsson, Winemaker, Sancheti, & Bhandari, 2014). Cartilage regeneration is not consistently effective in this age-group due to an impaired regenerative potential (Knutsen et al., 2007; Kreuz et al., 2006; Vanlauwe et al., 2011). TKA on the other hand, is not primarily indicated due to faster wear of prosthesis components in these relatively young patients and a subsequent high risk of revision surgery in the future (Li et al., 2014). Replacement of the osteochondral unit with an auto/allograft (Anderson, Robinson, Wiedrick, & Crawford, 2018; Baltzer, Ostapczuk, Terheiden, & Merk, 2016) or a focal knee resurfacing implant (FKRI) (Fuchs et al., 2018) does not rely on cartilage regeneration and could offer joint preservation. However, both auto- and allografting are hampered by drawbacks such as donor-site morbidity (Andrade et al., 2016) and limited availability (Gobbi, Scotti, Lane, & Peretti, 2015). FKRIs are an emerging group of implants typically intended for the treatment of cartilage defects in middle-aged patients, which may fill the treatment gap (Fuchs et al., 2018; Nathwani, McNicholas, Hart, Miles, & Bobic, 2017; Stalman et al., 2018).

Most FKRIs approved for clinical use are metal-based, comprising a highly polished cobalt-chromium articulating top to substitute cartilage and a titanium bone-substituting base (Fuchs et al., 2018; Pascual-Garrido, Daley, Verma, & Cole, 2017; Skoldenberg et al., 2014; Stalman et al., 2018). A primary prerequisite for FKRIs is adequate fixation in the subchondral bone, in order to maintain congruency to the articular surface (Martinez-Carranza et al., 2016; Stalman et al., 2018). Multiple studies have proven excellent osseointegration of titanium-based FKRIs (Custers et al., 2010; Martinez-Carranza et al., 2014; Stalman et al., 2018). However, there are concerns regarding the articulation of native cartilage with metal implants. Damage to the cartilage opposing the metal implant has been shown (Custers et al., 2010; Martinez-Carranza et al., 2016; Martinez-Carranza, Hultenby, Lagerstedt, Schupbach, & Berg, 2019), presumably as a result of the large mismatch between the mechanical properties of cartilage and the implant. Biomaterial advancements have led to the development of a hybrid implant comprised of a titanium base and a polymer top layer with an elastic modulus much more similar to the modulus of cartilage (Nathwani et al., 2017). However, the metal base still leads to scattering on computed tomography (CT) and magnetic resonance imaging (MRI) (Do, Sutter, Skornitzke, & Weber, 2018). Future clinical decision making is thus impaired, which is of great concern in case of new traumatic knee injuries (Adelani et al., 2016) and routine clinical follow-up of the knee joint.

Nondegradable thermoplastic polyurethane (TPU) is increasingly applied as a bearing surface in orthopaedic applications (Husby et al., 2016; Kanca, Milner, Dini, & Amis, 2018; Vrancken, Buma, & van Tienen, 2013) and is available in various Shore hardnesses (Sh). Bionate® II 80A (Sh) is the lowest stiffness medical grade Bionate® TPU, and approximates the compressive modulus of cartilage (Kanca et al., 2018). Bionate® 75D (Sh) is the highest stiffness medical grade

TPU and could potentially be used as a bone-substitute (Geary, Birkinshaw, & Jones, 2008). An osteochondral implant fully composed of TPU has the potential to overcome the typical drawbacks of metal-based implants, as it is MRI-compatible and theoretically would not lead to excessive stress in opposing cartilage (Heuijerjans, Wilson, Ito, & van Donkelaar, 2018; Kanca et al., 2018). Polymers however, pose specific challenges when implanted in bone. A low mechanical stiffness relative to bone can lead to micromotion between the implant and surrounding bone (Ma & Tang, 2014), which can subsequently lead to delayed healing, fibrous encapsulation and an inflammatory response with possible osteolysis (Gittens, Olivares-Navarrete, Schwartz, & Boyan, 2014). Consequently, there is no evidence of successful osseointegration of TPU to date.

The purpose of this study is to develop and evaluate a method to improve the osseointegrative potential of TPU. Next to the elastic modulus, numerous other factors contribute to implant osseointegration, such as the macro- and microscopic surface chemico-physical characteristics, initial implant stability, and the magnitude of applied loads (Parithimarkalaignan & Padmanabhan, 2013). Modification of the implant's bone-contacting surface roughness is a commonly described method to prevent implant fibrous encapsulation and achieve adequate implant osseointegration (Gittens et al., 2014). For titanium implants, a large body of literature supports the application of ≥ 1–2 μm R_a surface roughness to enhance osseointegration (Gittens et al., 2014; Wennerberg & Albrektsson, 2009), yet there is little data that confirms that these recommendations also apply to polymers (Deng et al., 2015; Suska et al., 2014). In addition, various polymer studies have demonstrated the necessity of surface functionalization using bioactive coatings (Cook et al., 2014; Deng et al., 2015; Remagen & Morscher, 1984). Polyethylene for instance, has been used as an unbacked acetabular cup in hip arthroplasty (Remagen & Morscher, 1984). Without coating, the polyethylene cup was shown to be encapsulated by fibrous tissue in humans upon *post mortem* analysis (Remagen & Morscher, 1984), whereas the addition of a calcium phosphate coating greatly enhanced its osseointegration in an animal trial (Gasser, Misteli, Eulenberger, Schonenberger, & Claes, 1996). Polyetheretherketone (PEEK) has a long-standing history as an interbody cage in spinal fusion, where the so-called "PEEK-Halo" is often observed (Phan, Hogan, Assem, & Mobbs, 2016). This phenomenon is indicative of a fibrous tissue interface between the spinal PEEK cage and vertebral bone (Phan et al., 2016). Preclinical studies have recently shown the beneficial effects of surface roughness modification and a calcium phosphate coating to promote osseointegration of PEEK (Deng et al., 2015; Suska et al., 2014). Calcium phosphate coatings such as hydroxyapatite (HA) and biphasic calcium phosphate (BCP) have been shown to accelerate implant-bone fixation and to lead to bridging of implant-bone voids of 1–2 mm for metal implants under stable mechanical conditions (Soballe et al., 1991). BCP has been successfully proven as a coating material to promote implant-bone bridging, and is therefore recommended for implant purposes (Dorozhkin, 2012).

In the current study, we hypothesize that surface roughness modification and application of a BCP coating to TPU implants will accelerate bone apposition and improve osseointegration. The first objective

of this study is to evaluate the effect of surface roughness modification and BCP-coating density variation of TPU discs on in vitro human bone marrow derived mesenchymal stem cell (hBMSC) viability and cell-mediated calcification. The second objective is to compare in vivo osseointegration of BCP-coated to uncoated TPU implants and titanium-based controls in a 12-week caprine large animal osteochondral model, as a proof of concept. The primary outcome measure of the in vivo study is the bone-to-implant contact area (BIC), determined through bone histomorphometrical analysis. Positron emission tomography PET/CT-scanning with the bone-seeking tracer ^{18}F sodium fluoride (^{18}F-NaF) is a nuclear modality that is able to nondestructively assess periimplant bone metabolism well before morphological changes are observed (Beheshti et al., 2015; Ullmark, Nilsson, Maripuu, & Sorensen, 2013). A secondary objective of the in vivo study is to visualize the bone metabolism surrounding to the implant using in vivo ^{18}F-NaF PET/CT-scanning at two timepoints and to determine whether this modality has a predictive discriminating potential for ultimate osseointegration.

2 | MATERIALS AND METHODS

2.1 | In vitro disc and in vivo implant manufacturing

Bionate® 75D (DSM Biomedical, Geleen, the Netherlands) TPU plates (80x80x2 mm) were injection moulded. Three different degrees of surface roughness were melt-pressed onto the plates with roughness based on the Verein Deutscher Ingenieure (VDI) 3,400 scale (Verein Deutscher Ingenieure, 1975): low-roughness (R_a 0.14 μm), medium-roughness (R_a 6.3 μm) and high-roughness (R_a 18 μm). Surface roughness applied to the TPU was evaluated using white light interferometry (Wyko NT1100, Veeco, New York, NY). Circular discs with a diameter of 20 mm were subsequently punched out. The surface roughness groups were then subdivided into three groups, each with a different degree of BCP coating: uncoated, double- or eight times dip-coated. Dip-coating was performed using a suspension of 5 wt% BCP particles (80% hydroxyapatite / 20% β-tricalcium phosphate, particle size distribution [d50] of 5.86 μm, CamBioCeramics, Leiden, the Netherlands) in tetrahydrofuran (1.09731, Merck, Kenilworth, NJ) without further additives. The suspension was made by vigorously stirring with a magnetic stirring bar, until shortly before use to prevent settling of particles. Dip-coating was performed by dipping the TPU discs in the BCP/THF suspension within 45 s after stopping of stirring. Double or eight times dipping was performed, with a drying time of 5 min between cycles. After the last dipping cycle, the discs were rinsed with ethanol and dried overnight at 40–60°C under vacuum. The two different BCP-coating densities were assessed using scanning electron microscopy. In total, nine types of TPU discs with varying surface modifications were evaluated: uncoated low-, medium-, and high-roughness TPU discs; double dip-coated low-, medium-, and high-roughness TPU discs; and eight times dip-coated low-, medium-, and high-roughness TPU discs. Titanium (Ti$_6$Al$_4$V) discs of the same

dimensions were manufactured and served as control. Titanium discs were corundum blasted to an approximate R_a of 2–3 μm (OHST Medizintechnik AG, Rathenow, Germany). All discs were sterilized using ethylene oxide, followed by aeration to remove residuals and then aseptically placed in 12-wells plates prior to the addition of culture medium and cells.

For the in vivo study, bilayered Bionate® TPU osteochondral implants were manufactured using a Xplore IM12 injection moulding machine (Xplore Instruments BV, Sittard, the Netherlands). The IM12 comprises a heated barrel to melt the polymer pellets, a piston to press the melted polymer from the barrel into a mould and a heated mould with inserts that determine the shape of the implant. Implants were cylindrical, measuring 8 mm in height and 6.1 mm in diameter. The articulating top layer (2 mm height) possessed a double-curvature to match the approximate respective sagittal and coronal curvatures of the goat knee, and was composed of Bionate® II 80A. The bottom layer (6 mm height) was composed of Bionate® 75D, and intended to osseointegrate with the subchondral/trabecular bone. Implants were produced in a two-step injection moulding procedure. In the first step, the top cavity was blocked with an insert that introduces macroscopic roughness to the interface layer to increase the interlocking surface for chemical and mechanical bonding, and only the bottom layers was moulded. Typically, about 5 g of Bionate® 75D pellets were melted at 235°C in the barrel. After 30 s the semimolten polymer was compressed to force out the air by applying a 4.5 bar pressure for 3 s. The bottom layer was then moulded using an 80°C mould temperature and 15 bar injection pressure for 2.2 s, followed by a packing pressure of 12 bar for 10 s. For the second injection-moulding step, the insert blocking the top cavity was replaced with an insert featuring a highly polished cavity for moulding the double-curvature top layer onto the bottom layer of the implant. About 5 g of Bionate® II 80A pellets were melted at 235°C for 5 min, including prepacking of the semi-molten polymer after 30 s. Then, the Bionate® II 80A was injected at 4.5 bar pressure for 5 s. The complete mould was taken from the machine and allowed to cool for 1–1.5 min to allow the Bionate® II 80A to solidify and prevent sticking and deformation of the material during removal of the full implant from the mould. After injection moulding, the implants were washed consecutively with water, ethanol, heptane, isopropanol, and again ethanol under ultrasonic conditions for 10 min. Finally, the implants were dried overnight at 80°C and reduced pressure (< 200 mBar) while maintaining a small N_2 flow. The surface topography of the Bionate® 75D layer was tailored based on the in vitro study results to enhance its osseointegration, see in vitro results (Section 3.2); VDI3400 medium-roughness was applied to the inside of the injection mould for fabrication of all TPU implants ($n = 16$). The Bionate® 75D bottom layer was dip-coated with BCP for half of the TPU implants ($n = 8$), while the other half ($n = 8$) was left uncoated. Implant dip-coating was performed for eight cycles in accordance with the method applied for the dip-coated discs. SEM analysis confirmed that a homogenous coating was attained, with a similar density as for the discs. After the last dipping cycle, the implants were rinsed with ethanol and dried overnight at 40–60°C under vacuum.

Metal control implants ($n = 8$) with analogous dimensions were manufactured (OHST Medizintechnik AG, Rathenow, Germany) with a

corundum blasted (R_a 2–3 μm) titanium (Ti_6Al_4V) stem and a polished (R_a < 0.05 μm) cobalt-chromium top.

All implants were double-packed and subsequently sterilized using ethylene oxide treatment, followed by aeration to remove residual ethylene oxide.

2.2 | In vitro cell viability and calcification assessment

2.2.1 | Cell culture

Human bone marrow derived mesenchymal stem cells (hBMSCs) from seven female adolescent donors were pooled and expanded to reach sufficient cell numbers (Institutional Review Board approval MUMC+ 08–4-056). Care was taken not to culture beyond passage five. Cells were plated at 5,000 cells/cm^2 in 1000 μl proliferation medium per well in 12-wells plates. Proliferation medium consisted of alpha-MEM (22–571-038, Thermo Fisher Scientific™, Waltham, MA), antibiotic-antimycotic 1% (v/v) (P4333, Sigma-Aldrich, Saint-Louis, MO) and EmbryoMax® ES Fetal Bovine Serum 10% (v/v) (EMD, Merck, Philadelphia, NJ). Cells were allowed to attach for 24 hr, and the proliferation medium was subsequently replaced by 1,000 μl osteogenic medium to differentiate the hBMSCs into the osteogenic lineage. The osteogenic medium consisted of proliferation medium supplemented with 10 nM dexamethasone (D8893, Saint-Louis, MO), 10 mM b-glycerol phosphate (50,020, Saint-Louis, MO) and 0.2 mM ascorbic acid 2-phosphate (A8960, Saint-Louis, MO). Osteogenic medium was refreshed every 2–3 days. HBMSCs were plated in three wells per biomaterial conditions, and two wells with only culture medium were included to control for background signal per biomaterial conditions. For the cell viability assay, a biomaterial-free well was also included as positive control.

2.2.2 | Cell viability

Cell viability was assessed after 24 hr in proliferation medium using PrestoBlue® (Thermo Fisher Scientific™, Waltham, MA). Cells were washed twice using phosphate buffered saline (PBS). Then, 100 μl PrestoBlue® reagent was added to 900 μl of fresh medium for each well and cultured for 4 hr. Samples of 100 μl PrestoBlue-cultured medium supernatant were measured in triplicate in microtiter plates using absorbance at 560 nm with reference wavelength set at 595 nm using a plate reader (Multiskan™ FC Microplate Photometer, Thermo Fisher Scientific™, Waltham, MA).

2.2.3 | Cell-mediated calcification

Cell-mediated calcification assessment was performed after 24 hr in proliferation medium and after 21 days in osteogenic medium using the Alizarin red-S assay. Alizarin red-S staining solution (ARS) was made by dissolving alizarin red-S dye (A5533, Sigma-Aldrich, Saint-Louis, MO) in dH_2O to a final concentration of 40 mM. The pH of ARS was set to 4.2 using ammonium hydroxide (338,818, Sigma-Aldrich, Saint-Louis, MO). Cells were washed three times using PBS and fixed in 10% (v/v) formaldehyde (47,608, Sigma-Aldrich, Saint-Louis, MO) at room temperature for 15 min. An excess of dH_2O was used to wash the cells after which the plates were allowed to air dry. ARS (1,000 μl) was added to each well. Plates with ARS were incubated at room temperature with gentle agitation for 30 min. Wells were washed five times using an excess of dH_2O, after which the discs were carefully inverted, and wells were washed again. Plates were allowed to air dry. In order to ensure complete dye extraction, discs were scraped, and the solution plus cells were transferred to a 1.5 ml microcentrifuge tube, vortexed for 30 s, and then covered with 500 μl mineral oil (M5904, Sigma-Aldrich, Saint-Louis, MO). The tubes were heated to 85°C for 10 min, transferred to ice for 5 min and then centrifuged at 20,000g for 15 min. Then, 500 μl of the supernatant was transferred to a fresh 1.5 ml microcentrifuge tube and 200 μl of 10% (v/v) ammonium hydroxide was added to neutralize the solution. 150 μl of the individual samples were subsequently spectrophotometrically analysed in triplicate at 405 nm absorbance in microtiter plates using a plate reader. A calibration series was taken along in these measurements. Absorbance of the samples was quantified to absolute bound Alizarin Red-S amount per disc, using the calibration series.

2.3 | In vivo Osseointegration assessment of Osteochondral implants

2.3.1 | Surgery

The animal trial protocol was approved by the central commission for animal testing (in accordance with the EU directive 2010/63/EU for animal experiments) and local animal welfare committee of Maastricht University (Project License: AVD107002016514). Twelve skeletally mature Dutch milk goats, aged 3.28 ± 0.49 years (mean ± SD) and weighing 84.75 ± 12.13 kg, were used for this study. Implants were bilaterally placed in the medial femoral condyles of the stifle joints of the goats. Block randomization was used to randomly assign the implants to the different knees (n = 24). Goats were allowed an acclimatization period of 2 weeks prior to surgery.

After intravenous injection of 10-20 mg/kg thiopental and endotracheal intubation, anaesthesia and analgesia was maintained by continuous administration of propofol (0.3–0.6 mg/kg/min) and sufentanyl (6 μg/kg/h). An intravenous bolus of 1–4 mg/kg propofol, and 5 μg/kg sufentanyl was initially administered. Prophylactic antibiotics (single dose of 1 g amoxicilline/clavulanic acid) were given 15 min prior to the incision. Both hind legs were shaved, disinfected using 0.5% (v/v) chlorhexidine, and covered using standard surgical sheets. A medial parapatellar incision was used to open the knee joint. Hoffa's fat pad was partially removed to increase visibility. A specifically designed Kirschner-wire guide was used to determine the angle perpendicular to the centre of the medial femoral condyle. A 2.4 mm

Kirschner-wire was drilled to serve as guide for the cannulated drill. A specifically designed depth-controller allowed for incremental increases of drilling depth, aiming at a flush to a slightly recessed implant position. After confirmation of the depth using an undersized dummy implant, the implant was unpacked and hammered into the defect. The wound was closed in layers using resorbable sutures. An overview of the most important surgical steps is provided in Figure 1a–d.

After recovering from anaesthesia, animals were allowed for immediate weight bearing. Postoperatively, pain medication consisted
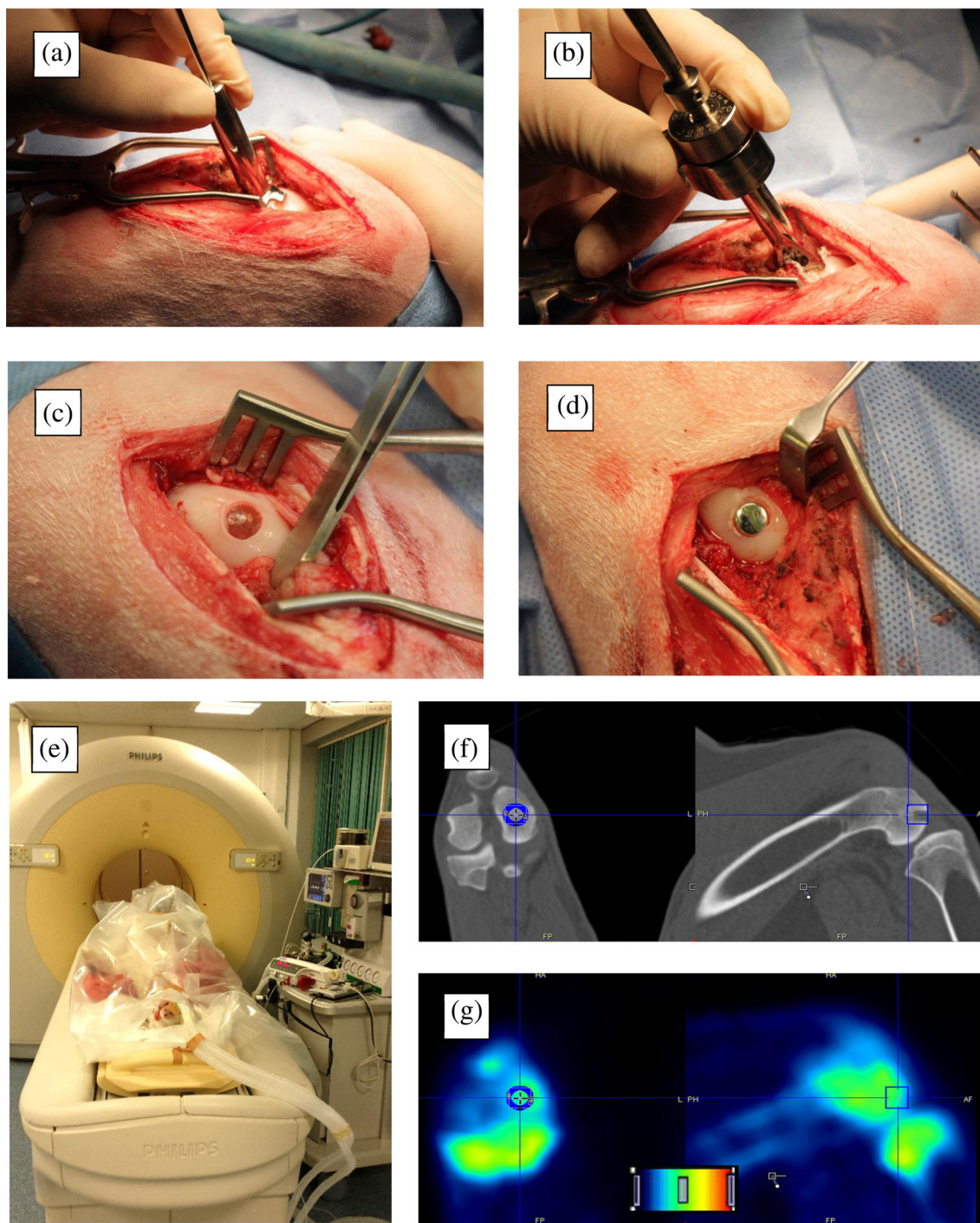
FIGURE 1 (a–d) Intraoperative steps of implantation: (a) Kirschner-wire guide with a footprint that matches the curvature of the goat knee for perpendicular implantation; (b) Depth-controller with cannulated drill inside for incremental steps of drilling depth; (c) thermoplastic polyurethane implant after implantation; and (d) metal implant after implantation; (e–g) Positron emission tomography CT-scanning of the goats and analyses: (e) Positioning and fixation of the anaesthetized goat in supine position; (f) The cylindrical volume of interest (VOI) measuring 10 mm in diameter and 15 mm in length is drawn in the diagnostic CT-scan. The bone is then isocontoured using a threshold value (not shown); (g) The VOI is then transferred to the static positron emission tomography image to obtain standardized uptake values in the bone within VOI

of intramuscular buprenorphine (5–10 μg/kg) and subcutaneous carprofen (2–4 mg/kg) injections for 3 days or longer if indicated. Subcutaneous amoxicillin/clavulanic acid (100 mg/ml, 1 ml / 20 kg) administration was continued for 5 days. The animals were housed in outdoor stables when sufficiently ambulant after surgery. Grain pellets, hay and water were provided ad libitum. The animal welfare officer continuously monitored the general health and care of the animals. Twelve weeks postsurgery animals were sacrificed by an intravenous pentobarbital overdose (200 mg/kg).

2.3.2 | Microscopic analysis of Osseointegration

After sacrifice, the knees were excised *en bloc* using a oscillating saw and subsequently dissected. The medial condyles were cut out, put in jars with neutral buffered formalin (NBF: formaldehyde 3,7% (v/v) in PBS), and stored on a rocking platform at 4°C for at least 2 weeks. Fixed specimens were dehydrated by incubation in increasing concentrations of ethanol in water up to 100% ethanol. Then, specimens were embedded in blocks using Epoxy resin (EpoThin 2, Buehler, Lake Bluff, IL) under vacuum. Resin blocks were cut using a band saw to orient the implants horizontally, and blocks were then mounted in a diamond saw (SP1600, Leica, München, Germany) using ultra low viscosity cyanoacrylate glue. A cut through the middle of the implant was made. Masson Goldner Trichrome (Carl Roth, Karlsruhe, Germany) staining was applied. Tissues were gently wiped dry and allowed to air dry for 5–10 min. A glass coverslip was glued to the tissue using cyanoacrylate glue. Sections of 50–70 μm were cut and glued to a glass slide with cyanoacrylate glue. The sections were scanned using bright light microscopy at a magnification of 200x (M8 Microscope, Precipoint, Freising, Germany). A custom written MATLAB script (MathWorks, Natick, MA) was used to determine the BIC, the percentage of the implant surface which is in direct contact with bone. This assessment was performed by two observers (RJ & AK), and the average values were used for comparison.

2.3.3 | Periimplant bone metabolism assessed by ¹⁸F-NaF PET/CT scans

PET/CT-scanning was performed at 3 weeks and 12 weeks after surgery under general anesthesia. PET and CT images were acquired with an integrated PET/CT scanner (Gemini TF 64 PET/CT, Philips, Eindhoven, the Netherlands). The goats were supine positioned on the PET/CT bed, while anesthesia was maintained. Sixty minutes after intravenous injection of 146–262.16 MBq (median 178.75 MBq) ^{18}F-NaF at 3 weeks, and 182.73–248.6 MBq (median 196.18 MBq) ^{18}F-NaF at 12 weeks, PET and CT images were acquired. After a low-dose CT acquisition scan of both knees (120 kV, 30 mAs, slice thickness 4 mm), a static PET scan of two bed positions of 5 min each was acquired. This was immediately followed by a diagnostic CT scan (64-slice helical, 120 kV, 250 mAs, slice thickness 1 mm, increment 0.8 mm). Scans were viewed on clinical software (EBW, Philips, Eindhoven, the Netherlands), and further analyzed using image quantification software (PMOD 3.0,

PMOD Technologies Ltd, Zürich, Switzerland). PET images were reconstructed into CT-based attenuation corrected images. The resulting bimodal ^{18}F-NaF PET/CT scans were evaluated. In each diagnostic CT scan, a cylinder of 10 mm in diameter and 15 mm in length was manually drawn surrounding the implant. A threshold was applied to the cylinder to obtain a volume of interest (VOI) that included the bone surrounding the implant. Figure 1e–g shows the animal position during PET/CT scanning and subsequent VOI computations. A control VOI was drawn in the fifth lumbar vertebrae (L5). The VOI's were subsequently transferred to the static PET image to obtain the standardized uptake value (SUV) within each VOI, by correcting the measured radioactivity concentration (A [kBq/ml]) in the VOI for the injected dose of ^{18}F-NaF (ID [MBq]) and the body weight of the goat (m [kg]) according to formula **(1)**. To correct for individual baseline bone metabolism of the goat, the maximum SUV values within each VOI were divided by the mean SUV values in the control region according to formula **(2)**, creating the corrected SUVmax (cSUVmax).

$$(\mathbf{1}) \; SUV = (A/(ID/m))$$

$$(\mathbf{2}) \; corrected\,SUVmax\,(cSUVmax) = ((SUVmax\,implant\,VOI)/ \\ (SUVmean\,lumbar\,vertebrae\,5)$$

PET/CT analyses were used to determine the change in cSUVmax between the two timepoints, the differences between the conditions, and correlation with histology.

2.4 | Statistical analyses

Statistical analyses were performed using SPSS 23 (IBM Analytics, New York, NY). Normal distribution was tested using Shapiro–Wilk test for all data. For the in vitro experiment, the one-way ANOVA was employed after the Levene's test confirmed equality of variance. The post hoc Bonferroni correction was used to determine the significant differences between each condition. For the bone histomorphometry and PET/CT scans, Student's T-test was used in case of normal distribution, and the Mann–Whitney *U*-test was used in case of nonnormal distribution. Interobserver reliability was assessed using the Crohnbach-alpha Intraclass Correlation Coefficient (ICC). ICC greater than 0.6 indicating good interobserver reliability. For all analyses, *P*-values lower than .05 were considered significant.

3 | RESULTS

3.1 | In vitro disc and in vivo implant manufacturing

The average R_a of the TPU discs after melt-pressing as assessed by white light interferometry was 0.12 μm, 8.40 μm and 22.72 μm for the low-roughness, medium-roughness and high roughness conditions respectively.

Dip-coating of the in vivo implants resulted on average in a weight increase of 1.7 (± 0.3) milligrams for a surface area of 128 mm^2 (13.3 ± 2.3 μg/mm^2). Figure 2 shows the different applied TPU surface modifications. Figure 3 shows the bilayered composition of the TPU implant and embedding of BCP particles.

3.2 | In vitro cell viability and calcification assessment

All uncoated, the double dip-coated medium- and high-roughness, and the eight times dip-coated high-roughness TPU discs showed significantly lower cell viability compared to the biomaterial-free condition (all $p < .05$). Cell viability of the biomaterial-free condition was not significantly different from the titanium and eight times dip-coated low- and medium-roughness TPU discs.

None of the tested conditions showed significant calcification after 24 hr. After 21 days, the medium-roughness uncoated TPU discs showed significantly more calcification compared to titanium ($p < .02$). The medium-roughness eight times dip-coated TPU discs showed significantly more calcification compared to the six other TPU conditions and titanium (all $p < .04$). All other biomaterial conditions did not lead to significantly increased calcification compared to other conditions. Figure 4 shows the graphs of the in vitro quantified cell viability and calcification results.

The TPU condition with the highest amount of calcification were selected as the optimal condition, and chosen to proceed in the in vivo study (see methods, section 2.1). Although the medium-rough uncoated TPU's showed decreased cell viability after 24 hr, this material was also
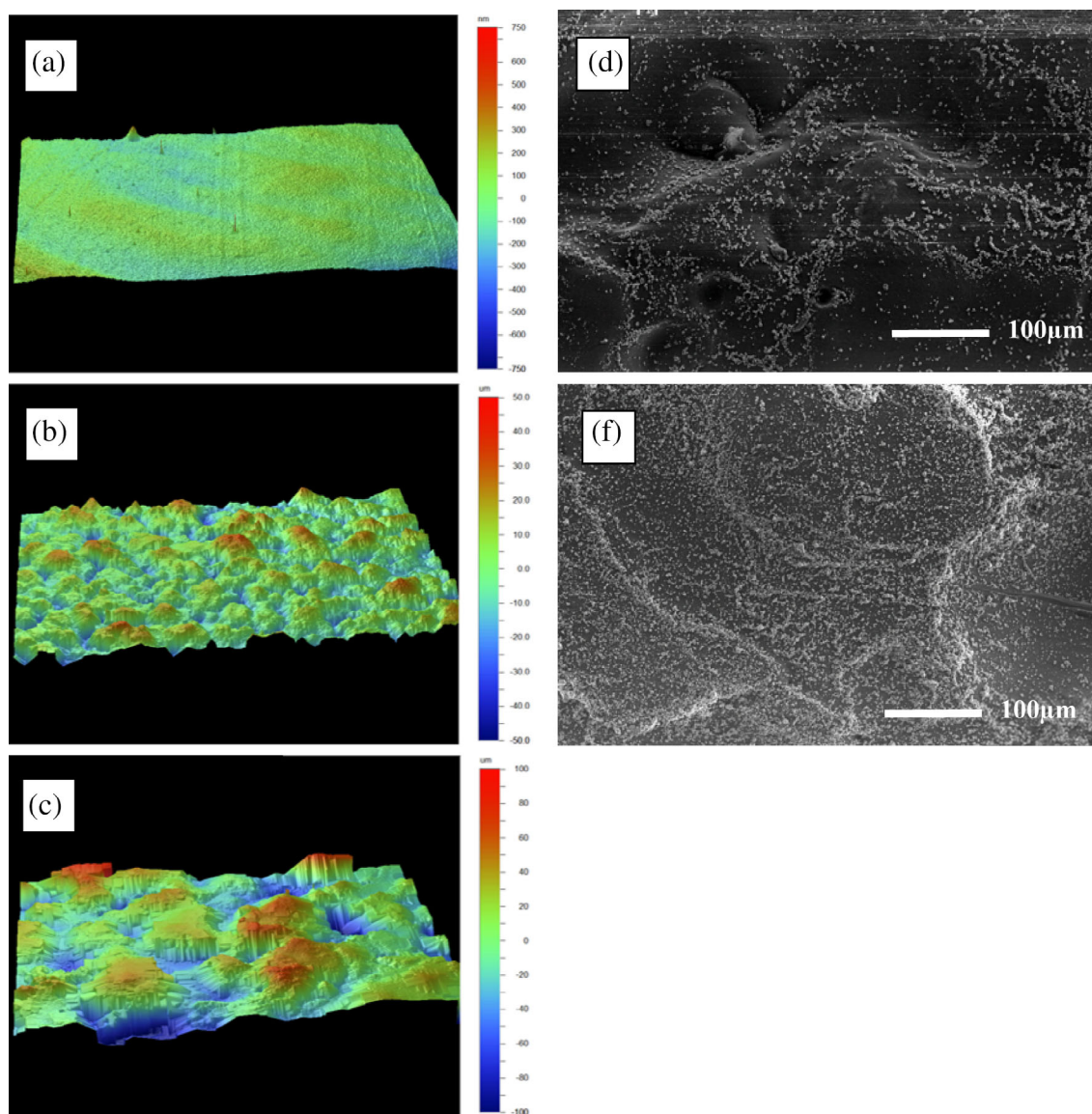
FIGURE 2 (a–c) White light interferometry analysis of thermoplastic polyurethane (TPU) plates after melt-pressing different degrees of surface roughness, showing an: (a) R$_a$ of 0.12 μm after melt-pressing with an R$_a$ 0.14 μm; (b) R$_a$ of 8.4 μm after melt-pressing with an R$_a$ 6.3 μm; (c) R$_a$ of 22.72 μm after melt-pressing with an R$_a$ 18.0 μm. (d,e) Scanning electron microscopy of TPU discs with an R$_a$ of 8.4 μm at a magnification of 200x after the TPU was: (d) double dip-coated with BCP particles in tetrahydrofuran; or (e) eight times dip-coated with BCP particles in tetrahydrofuran

FIGURE 3 (a) Schematic drawing of the implant; (b) Optical microscopy of an uncoated thermoplastic polyurethane (TPU) implant showing the bilayered construction of Bionate® (DSM Biomedical, Geleen, the Netherlands) II 80A and 75D and medium surface roughness with an R_a 8.40 µm; (c) Electron microscopy 5,000× magnification of a biphasic calcium phosphate (BCP) coated implant showing the BCP particles embedded on the TPU; (d) Electron microscopy 5,000× magnification of the same implant as in (c) after the BCP particles were dissolved using 1 M hydrochloric acid revealing crater-like holes which confirmed deep embedding of the particles in the TPU surface
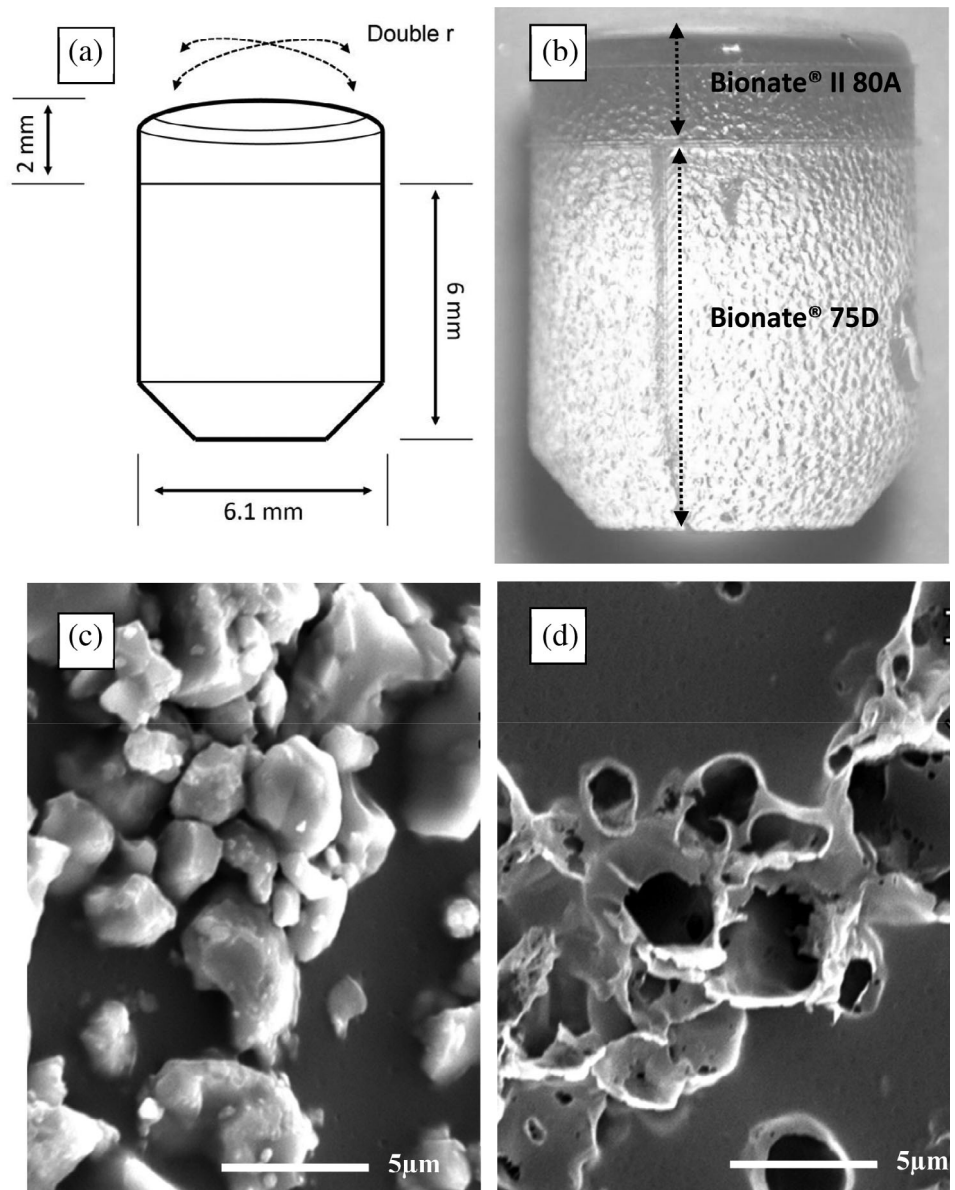
selected for implant manufacturing (see methods section 2.1.) to investigate the in vivo difference between uncoated and BCP-coated TPU with similar surface roughness.

3.3 | In vivo Osseointegration assessment of Osteochondral implants

3.3.1 | Animal health

All surgical procedures were successfully concluded, without occurrence of intraoperative complications. Animals regained normal gait 12 ± 7 (mean ± SD) days after surgery. Fourteen days after surgery, one of the animals started limping with one leg. Due to prolonged discomfort the animal was sacrificed (metal and uncoated TPU implant). Upon *post mortem* examination, it was discovered that suture resorption had led to medial retinaculum loosening and hence patellar

luxation. Two animals were prophylactically revised with nonresorbable sutures (Ethibond Excel, Ethicon, Johnson & Johnson Medical N.V. Belgium) after physical examination showed the ability to dislocate the patella laterally. One knee (metal implant) was not included for analysis due to a recurrent mild unilateral joint infection, which was subdued using antibiotic administration. Two animals suffered from superficial wound infections which resolved after antibiotic therapy. The weight change during the 12-week period was −7.7 ± 9.6 kg (mean ± SD). There were six metal, seven uncoated TPU implants and eight BCP-coated TPU implants remaining for evaluation at 12 weeks follow-up.

3.3.2 | Microscopic analysis of Osseointegration

None of the implants showed signs of loosening, both macroscopically, as well as upon probing after sacrifice. However, histology showed bone loss with fibrous encapsulation of the implant in two
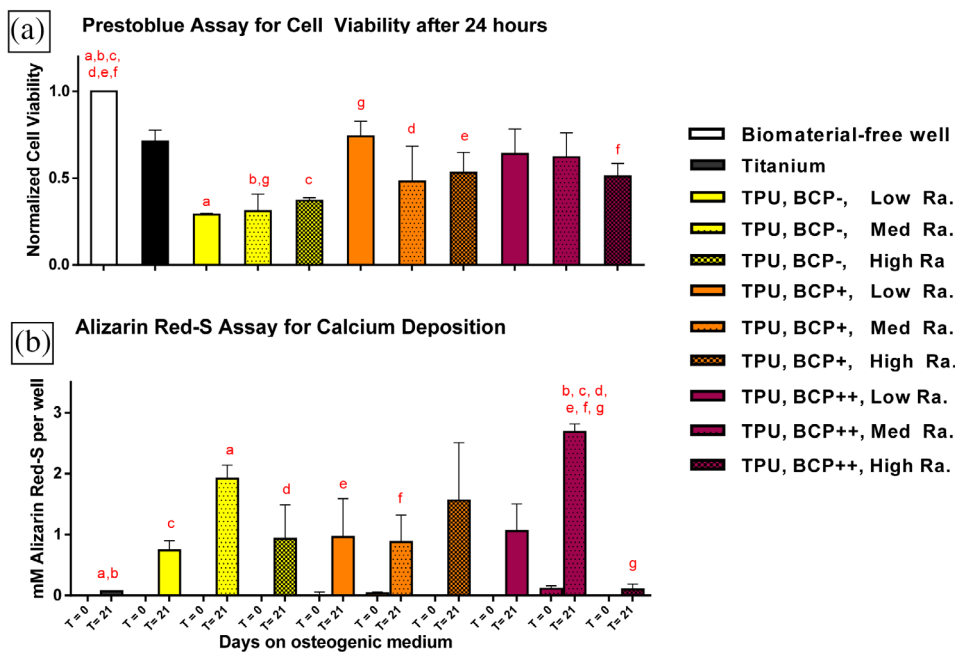
FIGURE 4 Thermoplastic polyurethane (TPU) discs with different surface modifications and corundum-blasted titanium control discs were tested in vitro. TPU surface modifications included three different degrees of surface roughness combined with three degrees of biphasic calcium phosphate (BCP)-coating; low R_a: low surface roughness R_a 0.12 μm; med R_a: medium surface roughness R_a 8.4 μm, high R_a: high surface roughness R_a 22.72 μm; TPU, BCP-: uncoated TPU; TPU, BCP+: double BCP dip-coated TPU; TPU, BCP++: eight times BCP dip-coated TPU. HBMSCs were plated and (a) Twenty-four hours after culture on proliferation medium cell viability was determined using a PrestoBlue assay. Results were normalized to the biomaterial-free well. (b) Additional discs with seeded hBMSCs were either sampled directly, or cultured for 21 days in osteogenic medium and calcification on the discs of both time points was colorimetrically quantified using an alizarin red-S assay. (a/b) Significant differences ($p < .05$) were determined using ANOVA and Bonferroni *post hoc* correction. A pair of similar alphabetic letters depicts a significant difference between two conditions

out of the six metal implants, three out of the eight BCP-coated TPU implants and six out of the seven uncoated TPU implants.

The BIC of 10.27 ± 4.50% (mean ± SD) for the BCP-coated TPU implants was significantly higher than the 4.50% ± 2.61 for the uncoated TPU implants ($p = .03$). The BIC of the uncoated TPU implants was significantly ($p = .04$) lower than the 12.81 ± 7.55% for the titanium in metal implants. There was no significant difference between BCP-coated TPU implants and the titanium in metal implants ($p = .68$). The ICC of the BIC assessment was excellent (0.868, $p = .00$). Typical examples of histological findings are shown in Figure 5a–c, and BIC-values are depicted in Figure 5d.

### 3.3.3 | Periimplant bone metabolism assessed by ^{18}F-NaF PET/CT scans

The cSUVmax values for the metal implants significantly decreased over time from 13.92 ± 2.21 (mean ± SD) to 4.34 ± 2.96 ($p = .04$). BCP-coated TPU implants followed a similar trend, with a decreasing cSUVmax from 9.13 ± 2.93 to 4.83 ± 2.76, although this decline did not reach statistical significance ($p = .07$). The cSUVmax for uncoated TPU implants decreased from 8.22 ± 2.89 to 6.47 ± 2.68, without statistical significance ($p = .31$).

At 3 weeks, the cSUVmax for the metal implants was significantly higher compared to the uncoated TPU implants ($p = .04$), but not significantly different from the cSUVmax for the BCP-coated TPU implants ($p = .10$). At 3 weeks, the cSUVmax was not significantly different between the BCP-coated and uncoated TPU ($p = .79$). At 12 weeks, the cSUVmax for all implant groups did not significantly differ from each other (All $p > .32$)). Figure 6 shows the cSUVmax values at 3 and 12 weeks.

The cSUVmax values at 3 weeks did not correlate to the BIC at 12 weeks (Pearson's R = .17, $p = .591$). There was a strong correlation between the cSUVmax values at 12 weeks and the BIC values at 12 weeks (Pearson's R = .74, $p = .001$).

4 | DISCUSSION

The purpose of this study was to develop and evaluate a surface modification and coating method to improve the osseointegration potential of TPU. The first goal was to assess the in vitro cell viability and cell-mediated calcification of different TPU surface modifications and coating densities. The addition of the eight times dipped BCP-coating combined with medium surface roughness (R_a 8.4 μm) did not have a negative effect on cell viability and resulted in significantly increased
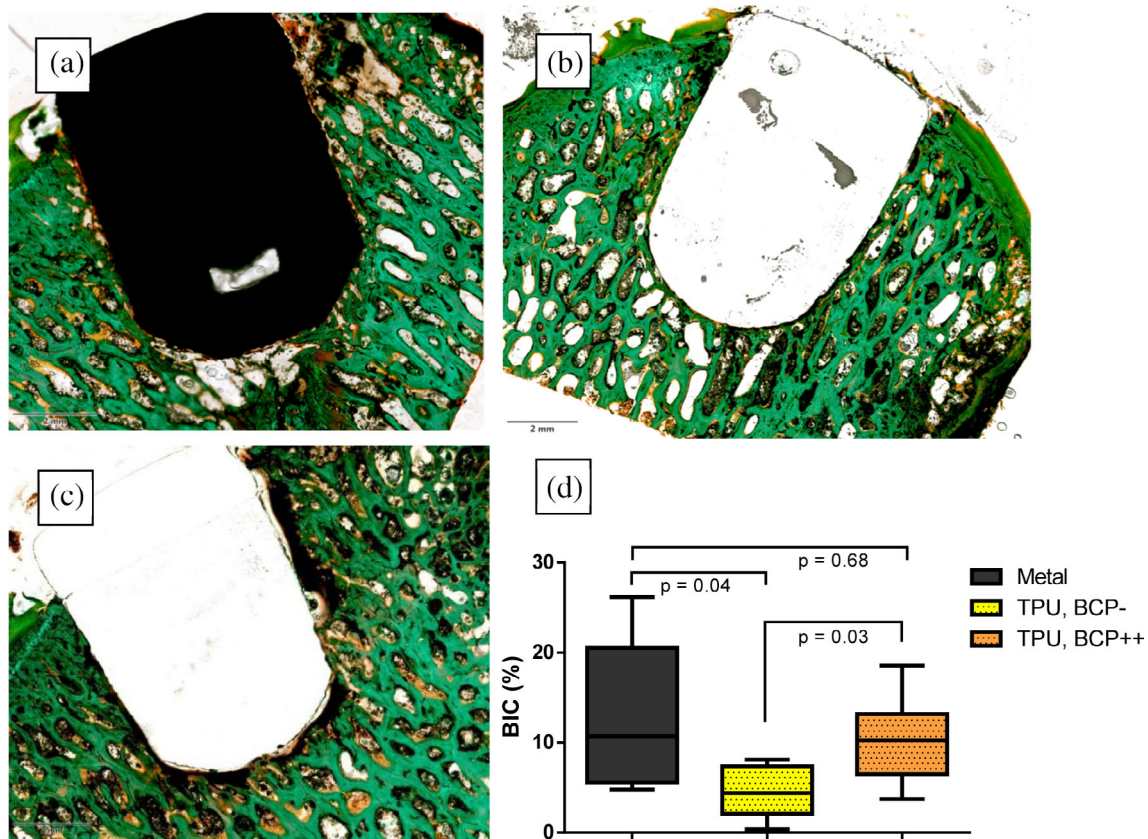
FIGURE 5 *Post mortem* assessment of implant osseointegration by bone histomorphometry: Coloured images show the typical nondecalcified histology examples of (a) metal implant; (b) biphasic calcium phosphate-coated thermoplastic polyurethane (TPU) implant; and (c) uncoated TPU implant. Note that for (a) and (b) there is bone directly in contact with the implant whereas in C there is a persistent gap between the implant and the surrounding subchondral bone with fibrous encapsulation of the implant. Graph (d): Boxplot showing the histomorphometry analysis of osseointegration of the three different implants using the bone-implant contact (BIC) percentage. TPU, BCP-: Thermoplastic polyurethane implants without coating. TPU, BCP++: Thermoplastic polyurethane implants with biphasic calcium phosphate coating. Given values are the average of two observers (intraclass correlation coefficient is .851)

in vitro cell-mediated calcification. The second goal was to assess in vivo osseointegration at the site of the intended FKRI application. Bone-implant-contact in the BCP-coated TPU implants was not significantly different from the titanium in metal implants, and was significantly higher in comparison to the uncoated TPU implants after 12 weeks. Comparing Week 3 and 12 ^{18}F-NaF PET/CT results, a similar pattern of declining ^{18}F-NaF tracer uptake was observed in the BCP-coated TPU and metal implants, indicating similar osseointegration processes.

This was the first study to investigate osseointegration of nondegradable TPU with surface modifications to improve osseointegration. Previous research on the osseointegration of titanium recommends the application of surface roughness with an R_a of approximately ≥1–2 μm (Gittens et al., 2014; Wennerberg & Albrektsson, 2009). Deng et al. (2015) applied an R_a of 1.96 μm on dental PEEK in accordance to these titanium recommendations and compared it to polished PEEK using a canine model. There was a significantly higher BIC after 8 weeks for the roughened PEEK compared to the polished condition. Suska et al. (2014) found high BIC values using either a HA or titanium coating on PEEK in an unloaded rabbit model. Surface roughness ranged

up to R_a 6.85 μm for the HA-coated PEEK. In the current study, an R_a of 8.4 μm was used which is relatively high in comparison to previous studies. However, comparison to the implants in the study by Deng et al. and Suska et al. is difficult due to use of different polymers, loading conditions and animal models. Further evidence on the effect of the variation of polymer surface roughness on osseointegration should be gathered before conclusive recommendations for polymer surface roughness application can be made. In addition, application of the BCP coating led to significantly better in vitro calcification and in vivo osseointegration compared to uncoated TPU. Based on the SEM analysis of the coated implants, we hypothesize that the dip-coating method allowed for sufficient dissolvement of the Bionate® 75D surface, allowing for partial enclosure of BCP particles for mechanical stability, while still allowing for biological interaction. Although calcium phosphate coatings are known to be relatively stable in body fluid and initiate apatite formation (Eliaz & Metoki, 2017), the mechanical strength and biological stability of the specific coating procedure in present study needs to be further evaluated.

The BIC magnitudes found in this study were in line with Custers et al. (2009), who investigated the use of oxidized zirconium FKRIs in
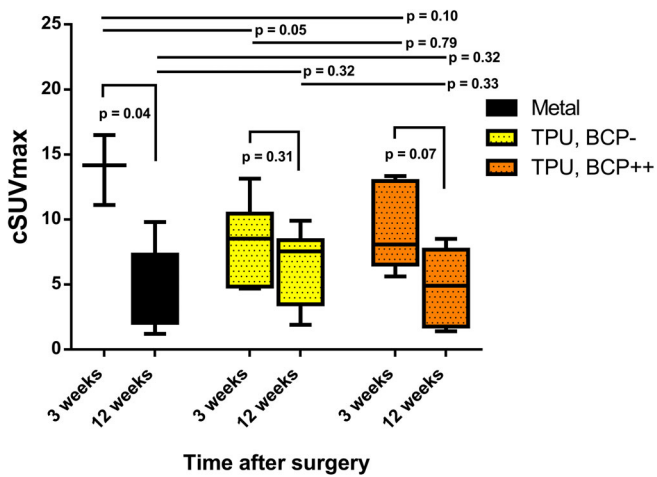
FIGURE 6 Periimplant corrected standard uptake value over time assessed by ^{18}F sodium fluoride positron emission tomography CT-scans: the corrected maximum standard uptake value (cSUVmax) of ^{18}F sodium fluoride in a designated bone volume of interest in the close proximity of the implants at 3 and 12 weeks after surgery are depicted. There was a statistical significant drop in cSUVmax over time for the titanium in metal implants, a similar trend for the biphasic calcium phosphate coated TPU implants (TPU, BCP++) and no statistical significant drop for the uncoated TPU implants (TPU, BCP-)

goats, and found a BIC of 14.6 ± 5.4% after 26 weeks. Uncoated PEEK has also been tested as bone-substitute in a canine FKRI study, but histological results showed socket expansion in 50% of the implants after 3 months, indicating severe osteolysis (Cook et al., 2014). FKRI studies with other implants have shown varying BIC magnitudes, but comparison is impossible due to much longer follow-up periods (Custers et al., 2007; Martinez-Carranza et al., 2014). Overall, higher BIC values are well-correlated with better mechanical stability of an implant (Haiat, Wang, & Brunski, 2014). Given this correlation, high BIC values should ideally be obtained at long-term to reassure permanent fixation. The interference fit of 0.1 mm for press-fit fixation used in this study was selected based on cadaver experiments (not shown), and enabled easy implantation, but may have allowed excessive micromotion. It is known that osseointegration is encouraged when less than 50 µm of micromotion occurs at the bone-implant interface (Udofia, Liu, Jin, Roberts, & Grigoris, 2007). Hence, a higher interference may be recommended in the future to further enhance osseointegration (Al-Marshood et al., 2011).

[18]F-NaF PET/CT-scans were obtained at 3 and 12 weeks in vivo. There was a strong correlation between bone histomorphometry and the cSUVmax at 12 weeks, which is in line with earlier findings (Messa et al., 1993). In the metal implant group, the cSUVmax was typically high at 3 weeks and then decreased significantly at 12 weeks. A similar trend was observed for the BCP-coated TPU implants, whereas this trend was not seen in the uncoated TPU implants. Ogawa et al. (2011) implanted titanium implants in the proximal tibial metaphysis in rats, and assessed the BIC and ^{18}F-NaF tracer uptake up to 25 days. All implants showed a BIC > 40% after 25 days, indicating good osseointegration in that study. An initial increase of ^{18}F-NaF

tracer uptake after surgery (t = 3 days) was also followed by a significant drop in ^{18}F-NaF tracer uptake at 25 days. The results of Ogawa et al. and the results in current study both indicate that successful implant osseointegration is characterized by a high initial ^{18}F-NaF tracer uptake with a relatively fast drop. Ullmark, Sorensen, & Nilsson (2012) demonstrated in a clinical study that ^{18}F-NaF PET/CT can also be used to distinguish in-growth patterns between HA-coated and uncoated acetabular cups after 1 week and 4 months. In the current study, there was a significant difference in cSUVmax between the metal and uncoated implants at 3 weeks. However, the 3-week cSUVmax values did not correlate to the BIC values at 12 weeks. We hypothesize that the effects of the surgical trauma were still too profound at 3 weeks to distinguish between biomaterial-related differences and variations in surgical trauma. Scanning at a later time point, such as 3 weeks postoperatively, would have been better suited to assess the predictive value of ^{18}F-NaF PET/CT as a nondestructive determination of osseointegration.

The strength of this proof-of-concept study was that it demonstrated the feasibility of achieving osseointegration of a TPU implant by means of surface modification and BCP-coating. There were also several limitations. The current in vitro set up was intended to allow for identification of the surface modification which provided the most cell-mediated calcification in order to select the most suitable candidate for the subsequent in vivo study. Although the in vivo study confirmed the in vitro findings, the osteoinduction and osteoconduction processes of BCP-coated TPU should be explored in future studies. Although BIC values and mechanical implant stability correlate well (Cappare et al., 2015; Scarano, Degidi, Iezzi, Petrone, & Piattelli, 2006), ex vivo pull-out tests could be obtained in future research and may provide a more clinical comparison between the different conditions. Another limitation is the unknown effect of the re-operations for patellar luxation in two goats on findings related to osseointegration.

The ultimate goal of FKRIs is postponing or eliminating the need for a TKA. This requires preservation of the opposing and adjacent tissues in the knee. If and to what extent a TPU implant is capable of preserving the native knee joint still needs to be determined. in vitro studies investigating the tribological effects of TPU against articular cartilage revealed low coefficient of friction values (Kanca et al., 2018; Majd et al., 2017), which decreased even further upon interaction with the synovial fluid proteins (Kanca et al., 2018). A preclinical goat study investigating a TPU artificial meniscal implant found no difference in histologic degenerative scores between the cartilages that articulated with the implant or against the native meniscus in the unoperated control knee after 6 months (Zur et al., 2011). Long-term follow-up FKRI studies are warranted to investigate the joint preserving potential of TPU.

In conclusion, osseointegration of BCP-coated TPU implants was not significantly different to titanium implants. TPU closely approximates the elastic modulus of articular cartilage, does not cause scattering on MRI or CT scans and can be tailored to enable osseointegration, rendering it is a promising candidate material for use in FKRIs. In contrast to metal, implants fully composed of nondegradable TPU with BCP-coating and surface modifications offer

a potential solution in the quest for a permanent, knee-preserving and imaging-compatible FKRI. The promising results of present study may also provide opportunities for further application of TPU in the field of bone and joint reconstruction in orthopaedic and trauma surgery. This proof-of-concept study justifies future investigations on the use of BCP-coated TPU implants.

CONFLICT OF INTEREST

This work was performed under the framework of Chemelot InSciTe. Two of the authors are employed by DSM Biomedical (RP, JT).

ORCID

Ralph M. Jeuken https://orcid.org/0000-0001-7729-8800
Alex K. Roth https://orcid.org/0000-0003-4121-8519

REFERENCES

Adelani, M. A., Mall, N. A., Brophy, R. H., Halstead, M. E., Smith, M. V., & Wright, R. W. (2016). The use of MRI in evaluating knee pain in patients aged 40 years and older. *The Journal of the American Academy of Orthopaedic Surgeons*, 24(9), 653–659.

Al-Marshood, M. M., Junker, R., Al-Rasheed, A., Al Farraj Aldosari, A., Jansen, J. A., & Anil, S. (2011). Study of the osseointegration of dental implants placed with an adapted surgical technique. *Clinical Oral Implants Research*, 22(7), 753–759.

Anderson DE, Robinson KS, Wiedrick J, Crawford DC. Efficacy of fresh Osteochondral allograft transplantation in the knee for adults 40 years and older. *Orthopaedic Journal of Sports Medicine* 2018;6(11): 2325967118805441, 232596711880544.

Andrade, R., Vasta, S., Pereira, R., Pereira, H., Papalia, R., Karahan, M., ... Espregueira-Mendes, J. (2016). Knee donor-site morbidity after mosaicplasty - a systematic review. *Journal of Experimental Orthopaedics*, 3(1), 31.

Baltzer, A. W., Ostapczuk, M. S., Terheiden, H. P., & Merk, H. R. (2016). Good short- to medium-term results after osteochondral autograft transplantation (OAT) in middle-aged patients with focal, non-traumatic osteochondral lesions of the knee. *Orthopaedics & Traumatology, Surgery & Research*, 102(7), 879–884.

Beheshti, M., Mottaghy, F. M., Paycha, F., Behrendt, F. F. F., Van den Wyngaert, T., Fogelman, I., ... Langsteger, W. (2015). (18)F-NaF PET/CT: EANM procedure guidelines for bone imaging. *European Journal of Nuclear Medicine and Molecular Imaging*, 42(11), 1767–1777.

Cappare, P., Vinci, R., Di Stefano, D. A., Traini, T., Pantaleo, G., Gherlone, E. F., & Gastaldi, G. (2015). Correlation between initial BIC and the insertion torque/depth integral recorded with an instantaneous torque-measuring implant motor: An in vivo study. *Clinical Implant Dentistry and Related Research*, 17(Suppl 2), e613–e620.

Cook, J. L., Kuroki, K., Bozynski, C. C., Stoker, A. M., Pfeiffer, F. M., & Cook, C. R. (2014). Evaluation of synthetic osteochondral implants. *The Journal of Knee Surgery*, 27(4), 295–302.

Curl, W. W., Krome, J., Gordon, E. S., Rushing, J., Smith, B. P., & Poehling, G. G. (1997). Cartilage injuries: A review of 31,516 knee arthroscopies. *Arthroscopy*, 13(4), 456–460.

Custers, R. J., Dhert, W. J., Saris, D. B., Verbout, A. J., van Rijen, M. H., Mastbergen, S. C., ... Creemers, L. B. (2010). Cartilage degeneration in the goat knee caused by treating localized cartilage defects with metal implants. *Osteoarthritis and Cartilage*, 18(3), 377–388.

Custers, R. J., Dhert, W. J., van Rijen, M. H., Verbout, A. J., Creemers, L. B., & Saris, D. B. (2007). Articular damage caused by metal plugs in a rabbit model for treatment of localized cartilage defects. *Osteoarthritis and Cartilage*, 15(8), 937–945.

Custers, R. J., Saris, D. B., Dhert, W. J., Verbout, A. J., van Rijen, M. H., Mastbergen, S. C., ... Creemers, L. B. (2009). Articular cartilage degeneration following the treatment of focal cartilage defects with ceramic metal implants and compared with microfracture. *The Journal of Bone and Joint Surgery. American Volume*, 91(4), 900–910.

Deng, Y., Liu, X., Xu, A., Wang, L., Luo, Z., Zheng, Y., ... Wei, S. (2015). Effect of surface roughness on osteogenesis in vitro and osseointegration in vivo of carbon fiber-reinforced polyetheretherketone-nanohydroxyapatite composite. *International Journal of Nanomedicine*, 10, 1425–1447.

Do, T. D., Sutter, R., Skornitzke, S., & Weber, M. A. (2018). CT and MRI techniques for imaging around orthopedic hardware. *Rofo*, 190(1), 31–41.

Dorozhkin, S. V. (2012). Biphasic, triphasic and multiphasic calcium orthophosphates. *Acta Biomaterialia*, 8(3), 963–977.

Eliaz, N., & Metoki, N. (2017). Calcium phosphate bioceramics: A review of their history, structure, properties, coating technologies and biomedical applications. *Materials (Basel)*, 10(4), 1–104.

Everhart, J. S., Abouljoud, M. M., Kirven, J. C., & Flanigan, D. C. (2019). Full-thickness cartilage defects are important independent predictive factors for progression to Total knee Arthroplasty in older adults with minimal to moderate osteoarthritis: Data from the osteoarthritis initiative. *The Journal of Bone and Joint Surgery. American Volume*, 101(1), 56–63.

Fuchs, A., Eberbach, H., Izadpanah, K., Bode, G., Sudkamp, N. P., & Feucht, M. J. (2018). Focal metallic inlay resurfacing prosthesis for the treatment of localized cartilage defects of the femoral condyles: A systematic review of clinical studies. *Knee Surgery, Sports Traumatology, Arthroscopy*, 26(9), 2722–2732.

Gasser, B., Misteli, F., Eulenberger, J., Schonenberger, U., & Claes, L. (1996). Mechanical and histological assessment of uncoated and HA- or Ti-coated PE and POM plugs implanted in rabbits. *Journal of Materials Science: Materials in Medicine*, 7(11), 651–656.

Geary, C., Birkinshaw, C., & Jones, E. (2008). Characterisation of Bionate polycarbonate polyurethanes for orthopaedic applications. *Journal of Materials Science. Materials in Medicine*, 19(11), 3355–3363.

Gittens, R. A., Olivares-Navarrete, R., Schwartz, Z., & Boyan, B. D. (2014). Implant osseointegration and the role of microroughness and nanostructures: Lessons for spine implants. *Acta Biomaterialia*, 10(8), 3363–3371.

Gobbi, A., Scotti, C., Lane, J. G., & Peretti, G. M. (2015). Fresh osteochondral allografts in the knee: Only a salvage procedure. *Annals of Translational Medicine*, 3(12), 164.

Haiat, G., Wang, H. L., & Brunski, J. (2014). Effects of biomechanical properties of the bone-implant interface on dental implant stability: From in silico approaches to the patient's mouth. *Annual Review of Biomedical Engineering*, 16, 187–213.

Heir, S., Nerhus, T. K., Rotterud, J. H., Loken, S., Ekeland, A., Engebretsen, L., & Aroen, A. (2010). Focal cartilage defects in the knee impair quality of life as much as severe osteoarthritis: A comparison of knee injury and osteoarthritis outcome score in 4 patient categories scheduled for knee surgery. *The American Journal of Sports Medicine*, 38(2), 231–237.

Heuijerjans, A., Wilson, W., Ito, K., & van Donkelaar, C. C. (2018). Osteochondral resurfacing implantation angle is more important than implant material stiffness. *Journal of Orthopaedic Research*, 36(11), 2911–2922.

Husby, K. A., Reed, S. K., Wilson, D. A., Kuroki, K., Middleton, J. R., Hoepp, N. C., ... Cook, J. L. (2016). Evaluation of a permanent synthetic Osteochondral implant in the equine medial femoral condyle. *Veterinary Surgery*, 45(3), 364–373.

Kanca, Y., Milner, P., Dini, D., & Amis, A. A. (2018). Tribological evaluation of biomedical polycarbonate urethanes against articular cartilage. *Journal of the Mechanical Behavior of Biomedical Materials*, 82, 394–402.

Knutsen, G., Drogset, J. O., Engebretsen, L., Grontvedt, T., Isaksen, V., Ludvigsen, T. C., ... Johansen, O. (2007). A randomized trial comparing autologous chondrocyte implantation with microfracture. Findings at five years. *The Journal of Bone and Joint Surgery. American Volume*, 89(10), 2105–2112.

Kreuz, P. C., Erggelet, C., Steinwachs, M. R., Krause, S. J., Lahm, A., Niemeyer, P., ... Sudkamp, N. (2006). Is microfracture of chondral defects in the knee associated with different results in patients aged 40 years or younger? *Arthroscopy*, 22(11), 1180–1186.

Li, C. S., Karlsson, J., Winemaker, M., Sancheti, P., & Bhandari, M. (2014). Orthopedic surgeons feel that there is a treatment gap in management of early OA: International survey. *Knee Surgery, Sports Traumatology, Arthroscopy*, 22(2), 363–378.

Ma, R., & Tang, T. (2014). Current strategies to improve the bioactivity of PEEK. *International Journal of Molecular Sciences*, 15(4), 5426–5445.

Majd, S. E., Rizqy, A. I., Kaper, H. J., Schmidt, T. A., Kuijer, R., & Sharma, P. K. (2017). An in vitro study of cartilage-meniscus tribology to understand the changes caused by a meniscus implant. *Colloids and Surfaces. B, Biointerfaces*, 155, 294–303.

Martinez-Carranza, N., Berg, H. E., Lagerstedt, A. S., Nurmi-Sandh, H., Schupbach, P., & Ryd, L. (2014). Fixation of a double-coated titanium-hydroxyapatite focal knee resurfacing implant: A 12-month study in sheep. *Osteoarthritis and Cartilage*, 22(6), 836–844.

Martinez-Carranza, N., Hultenby, K., Lagerstedt, A. S., Schupbach, P., & Berg, H. E. (2019). Cartilage health in knees treated with metal resurfacing implants or untreated focal cartilage lesions: A preclinical study in sheep. *Cartilage*, 10(1), 120–128.

Martinez-Carranza, N., Ryd, L., Hultenby, K., Hedlund, H., Nurmi-Sandh, H., Lagerstedt, A. S., ... Berg, H. E. (2016). Treatment of full thickness focal cartilage lesions with a metallic resurfacing implant in a sheep animal model, 1 year evaluation. *Osteoarthritis and Cartilage*, 24(3), 484–493.

Messa, C., Goodman, W. G., Hoh, C. K., Choi, Y., Nissenson, A. R., Salusky, I. B., ... Hawkins, R. A. (1993). Bone metabolic activity measured with positron emission tomography and [18F]fluoride ion in renal osteodystrophy: Correlation with bone histomorphometry. *The Journal of Clinical Endocrinology and Metabolism*, 77(4), 949–955.

Nathwani, D., McNicholas, M., Hart, A., Miles, J., & Bobic, V. (2017). Partial resurfacing of the knee with the BioPoly implant: Interim report at 2 years. *JBJS Open Access*, 2(2), e0011.

Ogawa, T., Zhang, X., Naert, I., Vermaelen, P., Deroose, C. M., Sasaki, K., & Duyck, J. (2011). The effect of whole-body vibration on peri-implant bone healing in rats. *Clinical Oral Implants Research*, 22(3), 302–307.

Parithimarkalaignan, S., & Padmanabhan, T. V. (2013). Osseointegration: An update. *Journal of the Indian Prosthodontic Society*, 13(1), 2–6.

Pascual-Garrido, C., Daley, E., Verma, N. N., & Cole, B. J. (2017). A comparison of the outcomes for cartilage defects of the knee treated with biologic resurfacing versus focal metallic implants. *Arthroscopy*, 33(2), 364–373.

Phan, K., Hogan, J. A., Assem, Y., & Mobbs, R. J. (2016). PEEK-halo effect in interbody fusion. *Journal of Clinical Neuroscience*, 24, 138–140.

Remagen, W., & Morscher, E. (1984). Histological results with cement-free implanted hip joint sockets of polyethylene. *Archives of Orthopaedic and Trauma Surgery*, 103(3), 145–151.

Scarano, A., Degidi, M., Iezzi, G., Petrone, G., & Piattelli, A. (2006). Correlation between implant stability quotient and bone-implant contact: A retrospective histological and histomorphometrical study of seven titanium implants retrieved from humans. *Clinical Implant Dentistry and Related Research*, 8(4), 218–222.

Skoldenberg, O., Eisler, T., Stark, A., Muren, O., Martinez-Carranza, N., & Ryd, L. (2014). Measurement of the migration of a focal knee resurfacing implant with radiostereometry. *Acta Orthopaedica*, 85(1), 79–83.

Soballe, K., Hansen, E. S., Brockstedt-Rasmussen, H., Hjortdal, V. E., Juhl, G. I., Pedersen, C. M., ... Bunger, C. (1991). Gap healing enhanced by hydroxyapatite coating in dogs. *Clinical Orthopaedics and Related Research*, 11(272), 300–307.

Stalman, A., Skoldenberg, O., Martinez-Carranza, N., Roberts, D., Hogstrom, M., & Ryd, L. (2018). No implant migration and good subjective outcome of a novel customized femoral resurfacing metal implant for focal chondral lesions. *Knee Surgery, Sports Traumatology, Arthroscopy*, 26(7), 2196–2204.

Suska, F., Omar, O., Emanuelsson, L., Taylor, M., Gruner, P., Kinbrum, A., ... Palmquist, A. (2014). Enhancement of CRF-PEEK osseointegration by plasma-sprayed hydroxyapatite: A rabbit model. *Journal of Biomaterials Applications*, 29(2), 234–242.

Udofia, I., Liu, F., Jin, Z., Roberts, P., & Grigoris, P. (2007). The initial stability and contact mechanics of a press-fit resurfacing arthroplasty of the hip. *Journal of Bone and Joint Surgery. British Volume (London)*, 89(4), 549–556.

Ullmark, G., Nilsson, O., Maripuu, E., & Sorensen, J. (2013). Analysis of bone mineralization on uncemented femoral stems by [18F]-fluoride-PET: A randomized clinical study of 16 hips in 8 patients. *Acta Orthopaedica*, 84(2), 138–144.

Ullmark, G., Sorensen, J., & Nilsson, O. (2012). Analysis of bone formation on porous and calcium phosphate-coated acetabular cups: A randomised clinical [18F]fluoride PET study. *Hip International*, 22(2), 172–178.

Vanlauwe, J., Saris, D. B., Victor, J., Almqvist, K. F., Bellemans, J., & Luyten, F. P. (2011). Tig/act, group EXTS. Five-year outcome of characterized chondrocyte implantation versus microfracture for symptomatic cartilage defects of the knee: Early treatment matters. *The American Journal of Sports Medicine*, 39(12), 2566–2574.

Verein Deutscher Ingenieure. Electrical Discharge Machining (DEM) - Definitions, processes, application. Verein Deutscher Ingenieure. Fachbereich Produktionstechnik und Fertigungsverfahren; 1975.

Vrancken, A. C., Buma, P., & van Tienen, T. G. (2013). Synthetic meniscus replacement: A review. *International Orthopaedics*, 37(2), 291–299.

Wennerberg, A., & Albrektsson, T. (2009). Effects of titanium surface topography on bone integration: A systematic review. *Clinical Oral Implants Research*, 20(Suppl 4), 172–184.

Zur, G., Linder-Ganz, E., Elsner, J. J., Shani, J., Brenner, O., Agar, G., ... Shterling, A. (2011). Chondroprotective effects of a polycarbonate-urethane meniscal implant: Histopathological results in a sheep model. *Knee Surgery, Sports Traumatology, Arthroscopy*, 19(2), 255–263.